16th World Conference on Earthquake, 16WCEE 2017

Santiago Chile, January 9th to 13th 2017

Paper N° 2055 (Abstract ID)

Registration Code: S-D1461871852

ANALYSIS OF MAGNITUDE-SPATIAL TRENDS OF INDUCED SEISMICITY IN OKLAHOMA, USA

R.K. McGuire(1), A. Zandieh(2), G.R. Toro(3)

(1) *Senior Principal, Lettis Consultants International, Inc., mcguire@lettisci.com*
(2) *Senior Engineer, Lettis Consultants International, Inc., zandieh@lettisci.com*
(3) *Senior Principal, Lettis Consultants International, Inc., toro@lettisci.com*

Abstract

Small earthquakes are occurring with a high rate in Oklahoma, USA, and have been attributed to ongoing fluid injection into the crust from disposal wells in the state. The rate of $m_b \geq 3$ is observed to be about 2 per day, or 730 per year, which exceeds the rate in California. Seismicity is occurring in central and northern Oklahoma, although fluid injection wells are distributed throughout the state. The largest recent earthquake in the region of high seismicity is the Pawnee, Oklahoma **M** 5.8 earthquake on September 3, 2016, which caused damage to multiple structures. Analysis of the b-value of small earthquakes since February 2014 indicates that b-values vary in time, ranging from about 1.0 to 3.0. Also, the temporal occurrences of larger micro-earthquakes ($m_b \geq 4.2$) appear to follow a peak in b-values. Finally, four moderate earthquakes (**M**$\geq$4.9) have occurred at the edges of the region of micro-seismicity. These effects are consistent with pore pressure changes from fluid disposal wells extending to larger distances with time, affecting favorably-oriented faults in adjacent areas, and triggering earthquakes on those faults. These effects can be replicated with a simple model of crustal pore pressure changes caused by fluid injection into a permeable geologic unit, with faults oriented randomly but close to a direction favorable to rupture under crustal stress conditions with small pore pressure changes, and with an exponential distribution of fault areas leading to an exponential distribution of earthquake magnitudes. Since January 2016 the rates of fluid injection in disposal wells have been restricted by Oklahoma state officials, so occurrences and characteristics of micro-seismicity in the region likely will change.

Keywords: induced seismicity; temporal seismicity changes

1. Introduction

The state of Oklahoma has experienced significant numbers of small-to-moderate seismicity since 2005, as shown in Fig. 1. There are a large number of fluid disposal wells permitted in Oklahoma to dispose of saline water generated by petroleum operations in the region (see Fig. 1). These wells dispose of fluids into the Arbuckle formation, a limestone and dolomite layer overlying basement rock. A possible connection between the seismicity and fluid disposal wells led the Oklahoma Corporation Commission to recommend reduction of fluid volumes [1, 2] in order to reduce the occurrence of earthquakes in the region.

An increase in seismicity in the central and eastern US has been observed since 2009 (Fig. 2). This increase in seismicity has been attributed to human activities, largely related to the petroleum industry [3]. The recent increase in seismicity in Oklahoma (Fig. 1) is consistent with this observation over the broader region of the central and eastern US.

This increase in seismicity has led to uncertainty in how to treat these small-to-moderate earthquakes when calculating national seismic hazard maps for the US. Figs. 3 and 4, published by the US Geological Survey (USGS) [4], shows alternative hazard calculation, both excluding the increased seismicity (Fig. 3), and including the increased seismicity (Fig. 4). To quantify the seismic hazard including the effects of this increased seismicity, the USGS has published a one-year seismic hazard forecast [5] that includes observed rates of small-to-moderate earthquakes in the central and eastern US.

With these observations of earthquake occurrences, it is useful to examine earthquake magnitudes and spatial trends, in order to gain a first-order understanding of the trends in seismicity and what might explain them. For that purpose we first examine the study area marked by the black square in Fig. 1, and analyze trends in seismicity with respect to magnitude, time, and location.

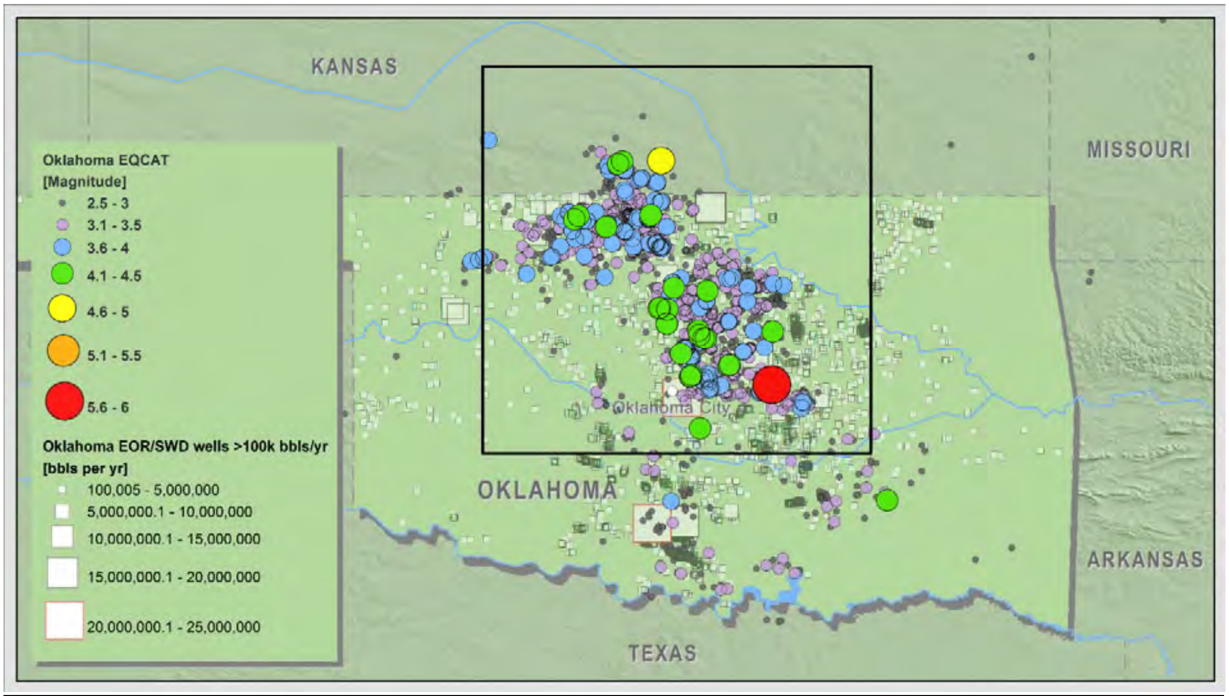

Fig. 1. – Earthquakes in Oklahoma, 2005-2014 (colored circles, colors representing earthquake magnitude), and locations of fluid disposal wells (white squares, size representing fluid volumes in barrels per year). Black square indicates area discussed in text. Earthquakes from USGS [4], well data from Weingarten *et al.* [6].

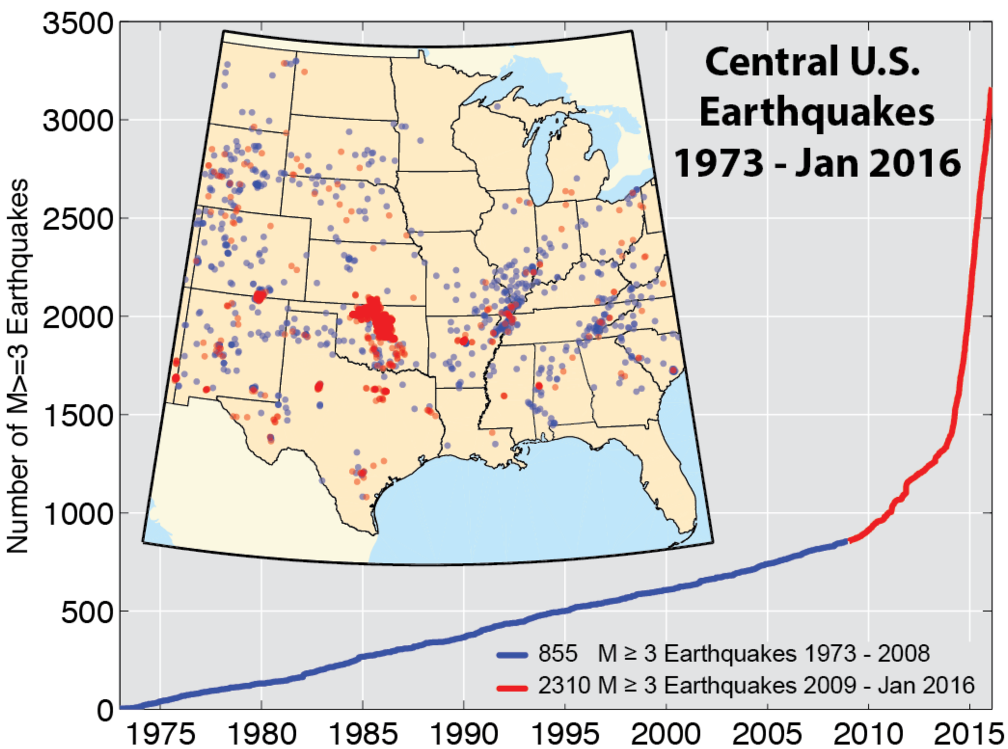

Fig. 2. – Cumulative number of M≥3 earthquakes in central and eastern US from 1973 to January 2016 [7]

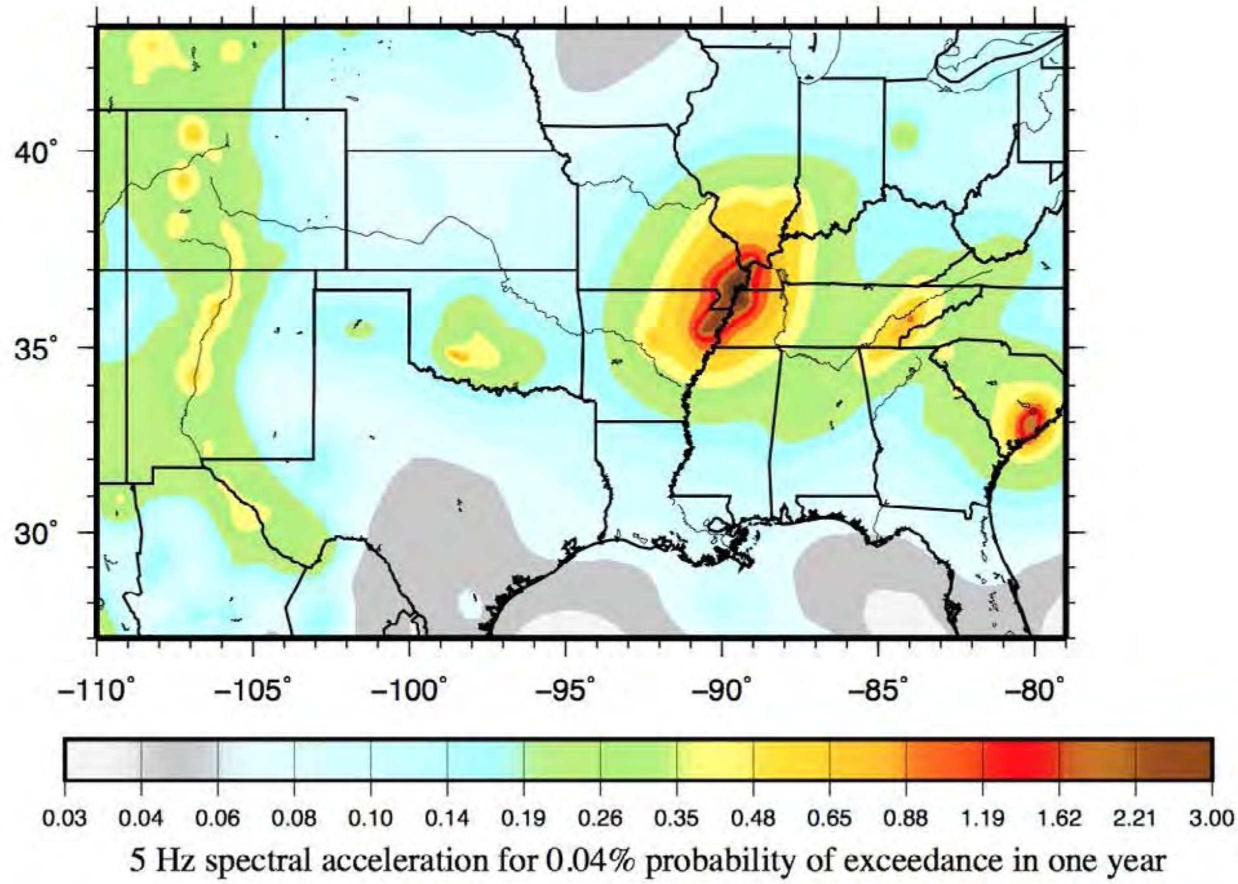

Fig. 3. – USGS seismic hazard map (5 Hz spectral acceleration, 0.04% annual probability of exceedance) for the central US, without including increased seismicity rates [8]. The high hazard in the central part of the map results from the New Madrid seismic zone, which experienced three M>8 earthquakes in 1811-1812.

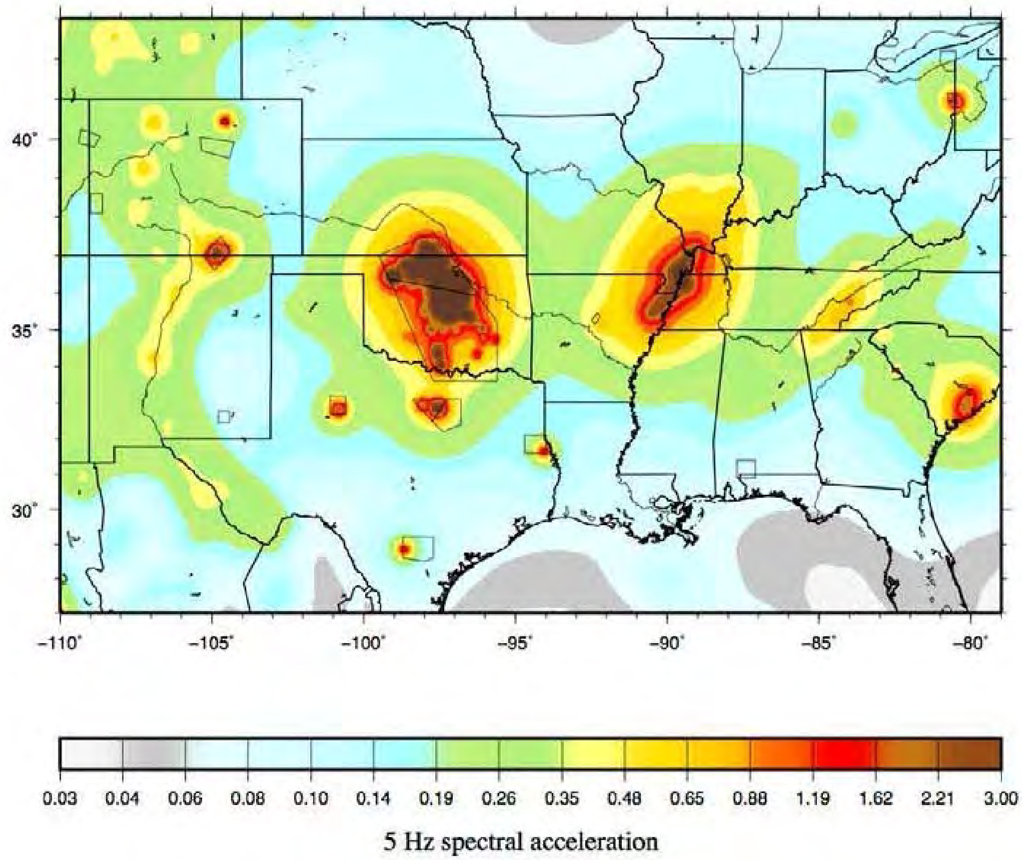

Fig. 4. – USGS seismic hazard map (5 Hz spectral acceleration, 0.04% annual probability of exceedance) for the central US, including increased seismicity rates [4]. The high hazard west of the New Madrid seismic zone results from increased seismicity rates, as shown in Fig. 2.

2. Earthquake occurrences in Oklahoma

Earthquake occurrences in the study area (see Fig. 1) are replotted in Fig. 5 for the period January 1, 2011—October 12, 2016. The locations and magnitudes are those reported by the Oklahoma Geological Survey [9] (OGS) and the USGS [10] for magnitudes $\geq$2.5. Note that several magnitude scales were used by the OGS and USGS for reporting these earthquakes (m_L, m_{bLg}, m_{wr}), and these are treated here as equivalent, for the purpose of examining trends in seismicity. Magnitude designations m_L, and m_b are designated "m" herein, magnitude designations m_w are designated "**M**" herein. Earthquakes occur in two clusters, one in central Oklahoma and a second in northwest Oklahoma. Fig. 6 plots earthquake hypocenters projected onto line A—A' (see Fig. 5). Earthquakes have been reported at a range of depths, from the surface to 12 km, with the majority of hypocenters reported from 2—8 km. The two distinct clusters of seismicity are evident in both Figs. 5 and 6. Red circles in Figs. 5 and 6 indicate the locations of four **M**$\geq$4.9 earthquakes that have occurred since January 1, 2011. Fig. 5 shows that all four **M**$\geq$4.9 earthquakes have occurred at the edge of the two seismicity clusters.

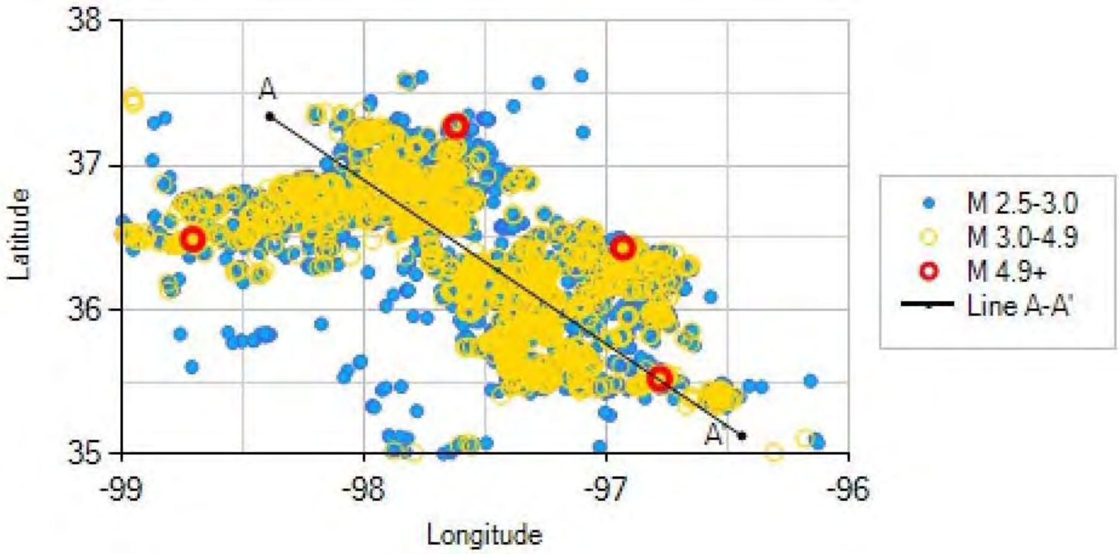

Fig. 5. – Map of earthquake epicenters in the study region from January 1, 2011—October 12, 2016, with color of circles indicating reported magnitude. Line A—A' is used to plot earthquake occurrences vs. depth (see Fig. 6). Red circles indicate locations of m≥4.9 earthquakes.

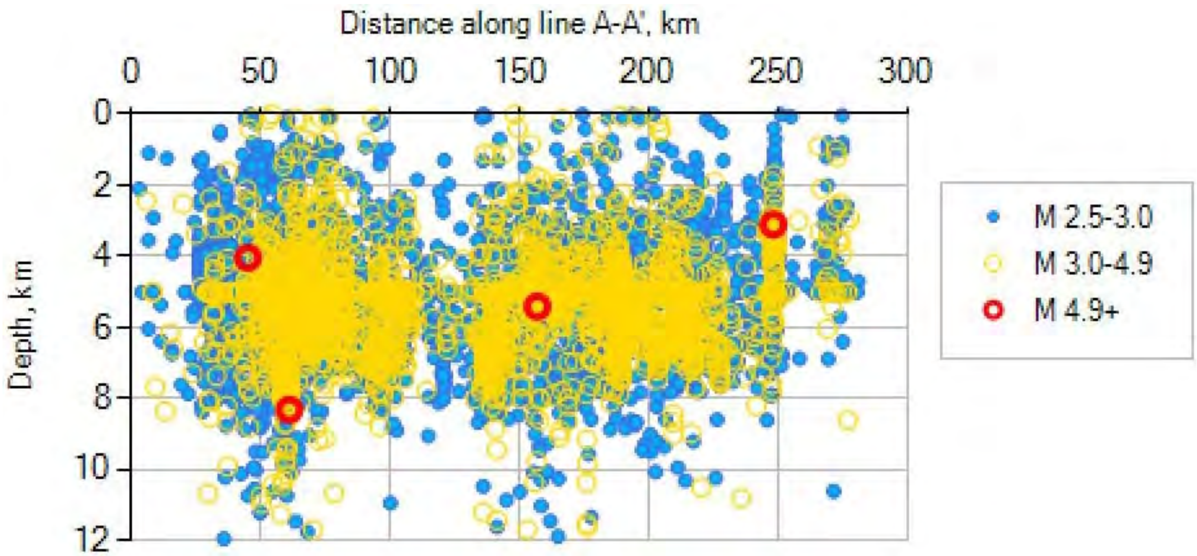

Fig. 6. – Earthquake hypocenters (see Fig. 5) projected onto line A—A' (northwest to southeast) vs. depth.

Fig. 8 shows a plot of numbers of earthquakes exceeding magnitude m (on logarithmic scale) vs. magnitude, which is a common "b-value" plot. The overall slope for m≥3.5 corresponds to a b-value of about 1.6, which is somewhat larger than a b-value of 1.0 that is common for tectonic earthquakes. Other researchers also observe a higher b-value for induced seismicity. For example, Mena et al [11] calculate b=1.47 for the induced earthquakes in Basel, Switzerland, in 2006. Other researchers observe a b-value of 1.0 or lower [12] for induced seismicity. In the current study, 2061 earthquakes with m≥3.0 occurred during the period between February 1, 2014 and October 12, 2016, which is an average of about 2 earthquakes per day. This is the time window used for further analysis, because prior to this window the rate of seismicity was lower, and October 12, 2016 corresponds to the deadline for preparation of this paper.

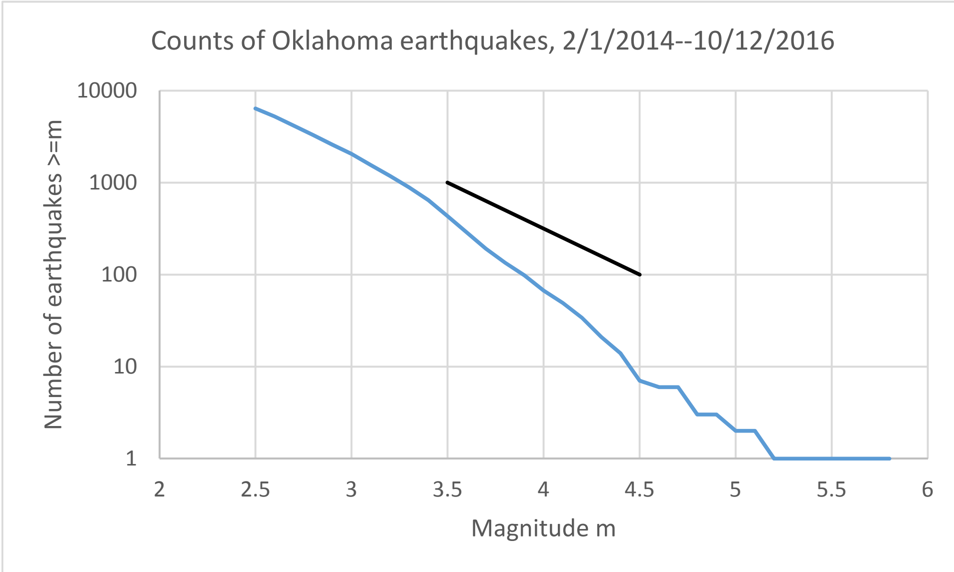

Fig. 7. – b-value plot of seismicity for the área shown in Fig. 5 from February 1, 2014—October 12, 2016. The average b-value for m≥3.5 is about 1.6. A b-value of 1.0 is shown with a black line for reference.

Fig. 8 shows b-values (blue line) calculated for m≥3.0 earthquakes (using the maximum likelihood method) for a 20-day window and overlapping 5-day time steps vs. time, and also shows the rate of earthquake occurrences (green line) with that same window and time step vs. time, for the period February 1, 2014—October 12, 2016. The b-values (blue line) indicate an overall average near 1.6, as seen in Fig. 7, with wide variations from values less than 1.0 to values greater than 3. The rate of earthquake occurrences (green line, right scale in Fig. 8) indicates an average rate of 2 earthquakes per day, with wide variations from 1 to more than 4 earthquakes per day.

Also shown on Fig. 8 are vertical red lines corresponding to the time of occurrence of m≥4.2 earthquakes. Individual magnitudes for these earthquakes are indicated near the top and bottom of each red line. One trend that is observed is that m≥4.2 earthquakes tend to occur in time after peaks in b-values. This correlation has been noted in Oklahoma by other researchers [13]. Fig. 9 plots b-values calculated using the same data and parameters as shown in Fig. 8, with a range of time windows and time steps. This demonstrates that the correlation is not an artifact of a specific choice of time window and time step. Other researchers have concluded that variations in b-value in time for induced earthquakes are significant. For example, Convertito et al [14] plot b-values in time for the Geysers geothermal field and conclude that, "Because the (minimum magnitude of completeness) values are stable within these (time) periods, these observed trends in the b-values can be considered as real features of the induced seismicity." Also, Martinez-Garzon et al. [15] conclude that "…increases in fluid injection rates…coincide with decreases in b-values (for the Geysers geothermal field)."

There is, of course, some statistical uncertainty in b-value calculated from a limited dataset obtained from a 20-day window of seismicity. When seismicity rates are high (above 2 earthquakes per day in Fig. 8), the statistical standard deviation in b-value is about 0.24. When seismicity rates are low (near 1.5 earthquakes per day in Fig. 8), the statistical standard deviation in b-value is about 0.29. Also, peaks in b-values appear to correlate with lows in seismicity rate in Fig. 8, which is consistent with seismicity responding to changes in volumes and pressures of underground fluid disposal. It does not appear that the characteristics of earthquakes in adjacent time windows are independent, these earthquakes are related to slow changes in crustal stress conditions, so observations in one time window may give insights into earthquake occurrences in subsequent time windows.

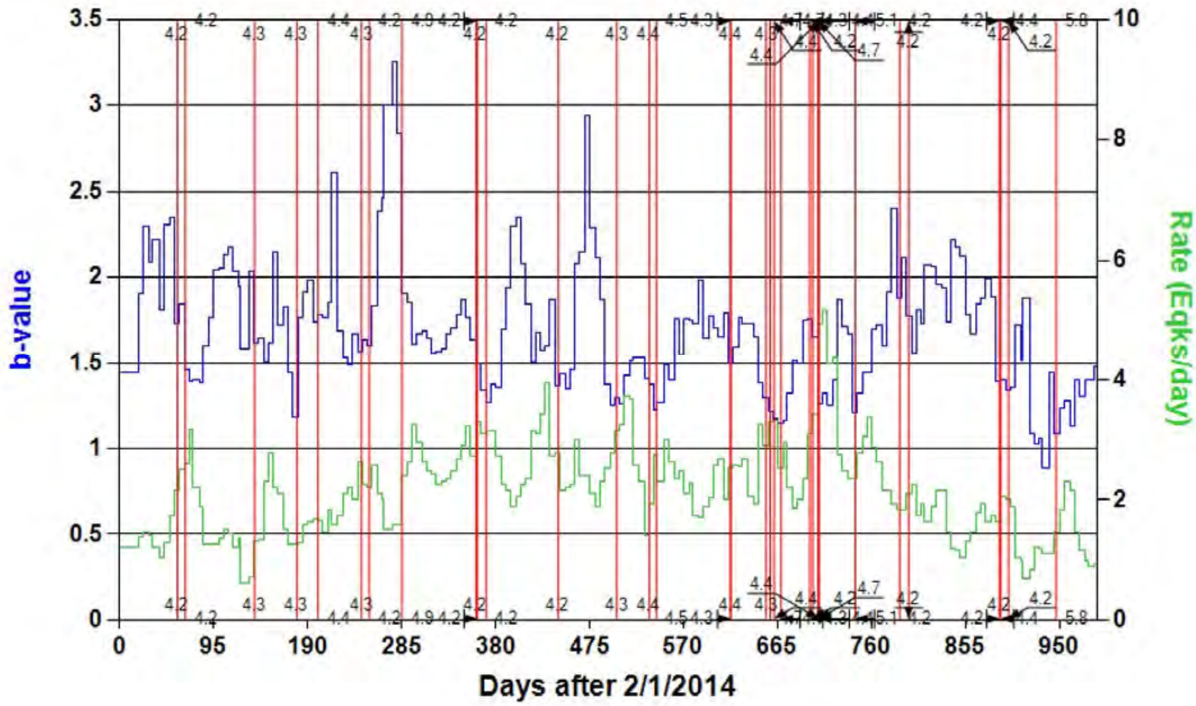

Fig. 8. – b-value (blue line) and seismicity rate (green line) vs. time for earthquakes with m≥3.0, using a 20-day window and a 5-day time step for the period February 1, 2014—October 12, 2016. Red lines indicate occurrences of earthquakes with m≥4.2.

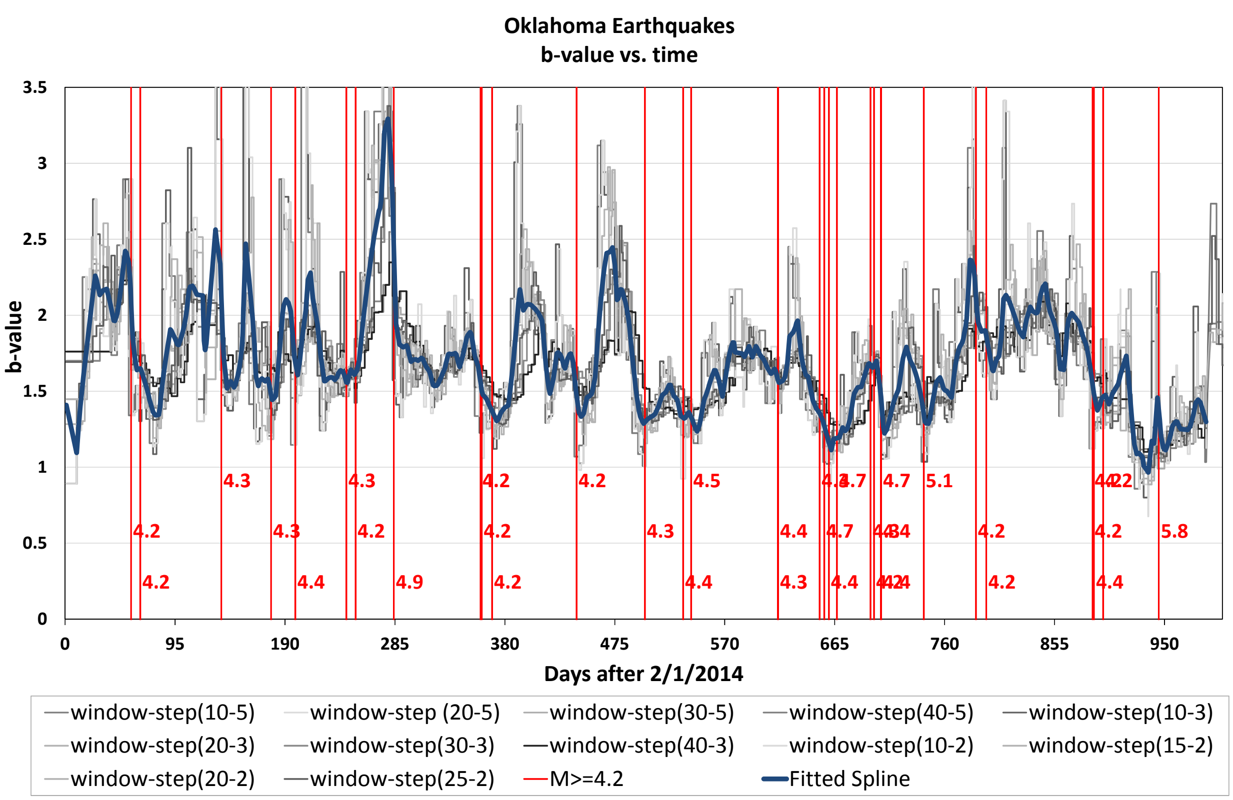

Fig. 9. – b-value vs. time for Oklahoma seismicity, February 1, 2014—October 12, 2016 for different time windows and time steps. Red lines indicate occurrences of earthquakes with m≥4.2.

Another important observation of the seismicity in Oklahoma is that moderate earthquakes (defined here as **M**≥4.9) tend to occur at the edges of seismicity clusters, rather than within the clusters. This is illustrated in Fig. 5, which plots **M**≥4.9 earthquakes along with all seismicity reported from 1/1/2011 to 10/12/2016. A more detailed summary is shown in Figs. 10A through 10D, which plot the four earthquakes with **M**≥4.9 along with the seismicity reported in the previous 20 days. Each of these 4 moderate earthquakes occurred near the edge of seismicity recorded during the prior 20 days.

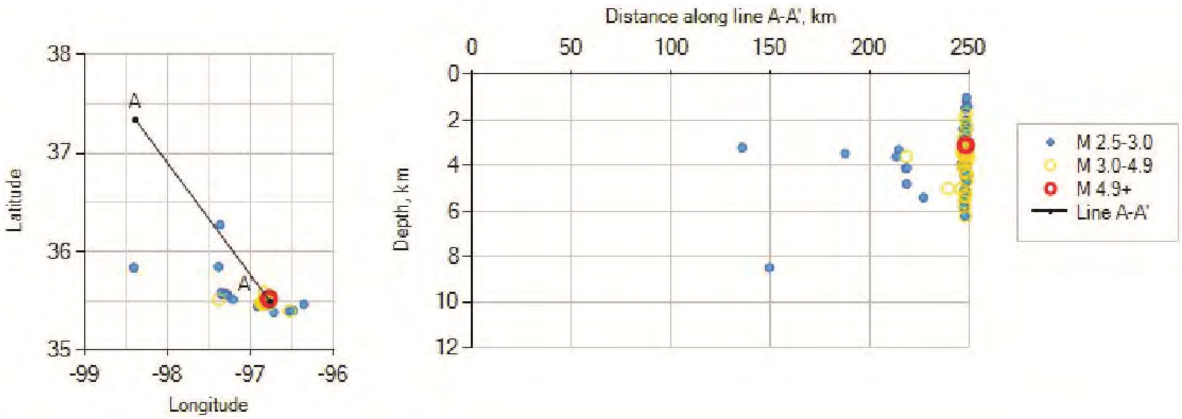

Fig. 10A. – Map (left) and projection onto line A-A’ (right) showing **M**5.7 earthquake that occurred on November 6, 2011 and seismicity reported in 20 days prior to that earthquake.

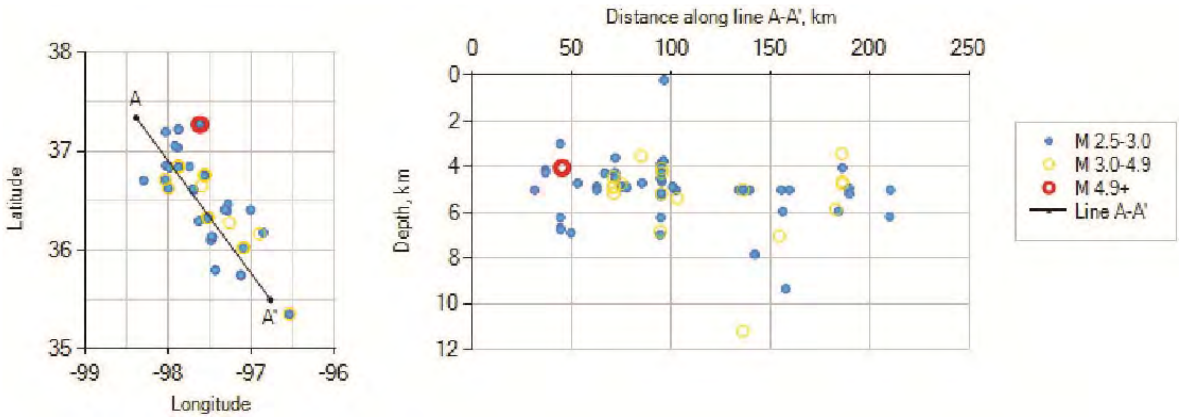

Fig. 10B. – Map (left) and projection onto line A-A’ (right) showing **M**4.9 earthquake that occurred on November 12, 2014 and seismicity reported in 20 days prior to that earthquake.

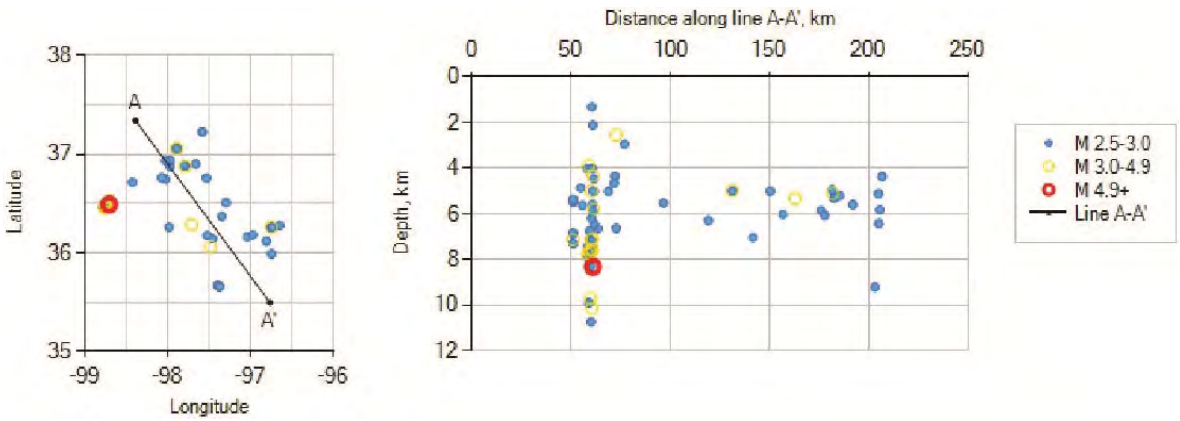

Fig. 10C. – Map (left) and projection onto line A-A’ (right) showing **M**5.1 earthquake that occurred on February 13, 2016 and seismicity reported in 20 days prior to that earthquake.

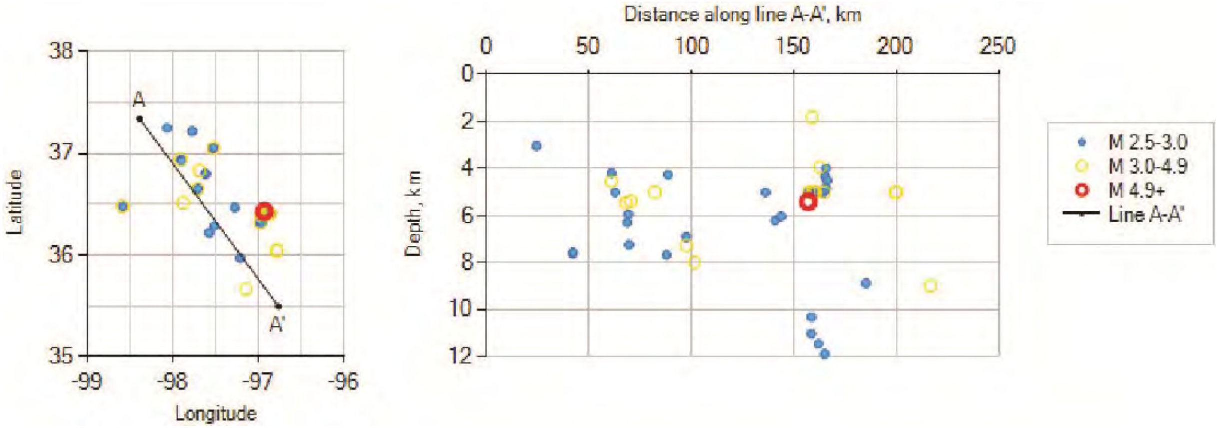

Fig. 10D. – Map (left) and projection onto line A-A' (right) showing **M**5.8 earthquake that occurred on September 3, 2016 and seismicity reported in 10 days prior to that earthquake.

3. Modeling earthquake occurrences in space and time

To gain insight into possible physical processes that might relate earthquake occurrences to the injection of fluid, we developed a simple model with the following characteristics.

Pore pressure. A simple Darcy flow model was used to calculate pore pressure from fluid injection into a geologic unit, with assumed (arbitrary) values of permeability, porosity, and thickness of the geologic unit, assumed (arbitrary) volumes of water injected, and viscosity and compressibility typical of water. Pore pressure was calculated as a function of time and distance from the injection point. This calculation conceptually represents disposal of saline water into a high-permeability formation such as the Arbuckle unit in Oklahoma, which is of lower Ordivician age.

Crustal characteristics. The earth's crust was modeled with maximum and minimum principal stresses that gave a typical critical angle between maximum principal stress and fault orientation. Faults on which earthquakes could occur were modeled in space using random (simulated) fault orientations that were close to the critical orientation for failure, given the principal stresses. Some faults were modeled with random (simulated) areas, to obtain an exponential distribution of earthquake magnitudes between 3.0 and 4.5 with a b-value of 1. Other faults were modeled to represent rupture areas producing magnitudes between 4.5 and 6, with an exponential distribution and b-value of 2. Aftershocks were modeled on ruptured faults with magnitudes smaller than main shocks occurring on the same fault with magnitudes one-half unit less than the main shock, in the subsequent time window. The results presented here do not depend on details of the aftershock model. Ruptured faults were assumed to create a pathway of increased permeability to adjacent locations, which then had the possibility of triggering favorably oriented faults at later times. This conceptually represents pore pressure changes in the permeable disposal formation being transferred to the underlying pre-Cambrian basement rock, and fault ruptures in the basement rock also rupturing the overlying disposal formation, creating high-permeability pore fluid pathways that can affect adjacent cells in the model.

Earthquake occurrences. Pore pressure changes were calculated for spatial cells representing the basement rock surrounding the injection well, and triggering of earthquakes was determined if the pore pressure change in each cell was sufficient, using a Mohr-Coulomb failure criterion, to cause rupture on the fault in that cell with its simulated orientation. If a fault rupture was triggered, the magnitude of the earthquake was determined by the simulated area of the fault. Faults do not rupture multiple cells, but ruptures can affect adjacent cells as described above.

Results. Pore pressure calculations were made, and earthquakes were simulated using the above-described model, for a period of 600 days and a distance of 8 km from the injection well. The distance of 8 km is smaller than the earthquake clusters illustrated in Fig. 5 (dimension of ~100 km) because the illustrative model uses only 1 disposal well, but the number of disposal wells in Oklahoma is large (Fig. 1). During the 600-day period, pore-pressure changes and earthquake occurrences were simulated using non-overlapping 20-day time windows. Fig. 11 shows a plot of one simulation, illustrating that earthquakes occurring soon after injection starts tend to be located at all distances to the well, but earthquakes at later times tend to be located at farther distances. This is consistent with the pressure plume traveling farther with time and with pore pressures increasing more (on a percentage basis) with time at farther distances.

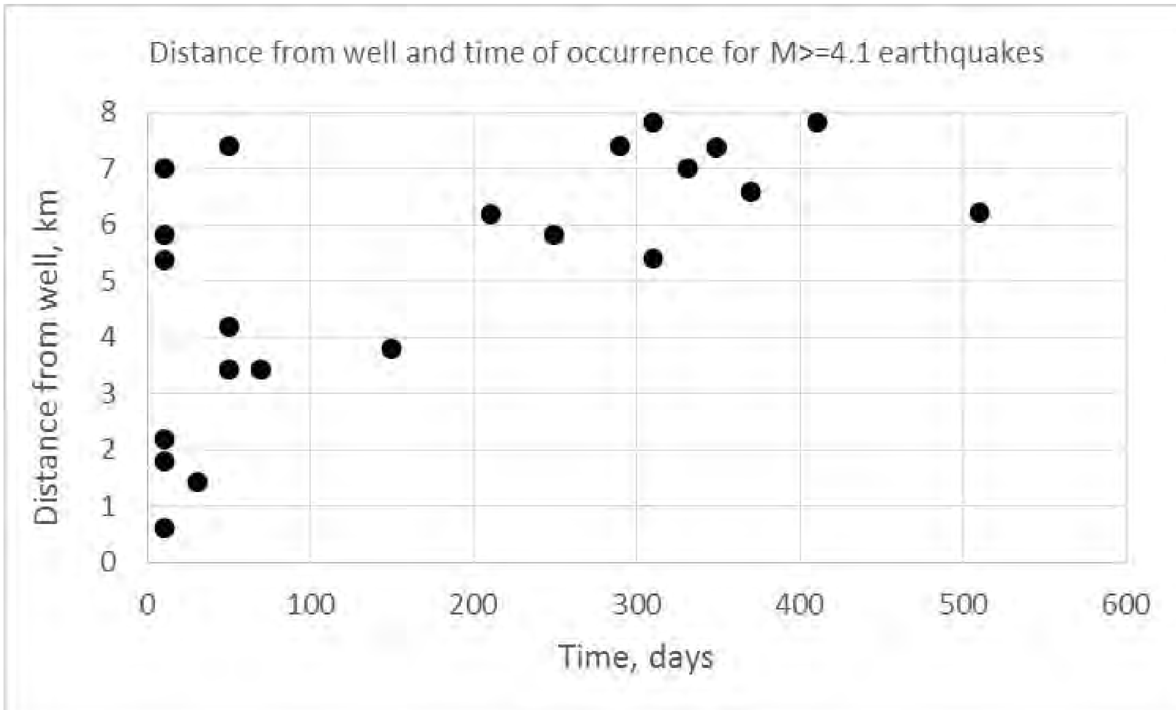

Fig. 11. – Simulated earthquake occurrences for M≥4.1 showing distance from injection well vs. time.

Fig. 12 shows a plot of the same simulated earthquakes with M≥4.1 in time, and calculated b-values for 2 sets of earthquakes occurring in the simulation: mainshocks only, and mainshocks plus aftershocks. Many earthquakes occur at early times (in the first 200 days) because pore pressure is changing quickly due to the onset of injection and the system produces many M≥4.1 earthquakes. Fig. 12 indicates that, after t=200 days, the occurrences (in time) of M≥4.1 earthquakes tend to follow high b-values, whether the b-value is calculated with or without aftershocks. For the peaks in b-value shown in Fig. 12, the b-value for mainshocks plus aftershocks (which is also what is plotted in Fig. 8) decreases prior to the occurrence of M≥4.1 earthquakes, indicating that the low b-values are not just the result of M≥4.1 earthquakes.

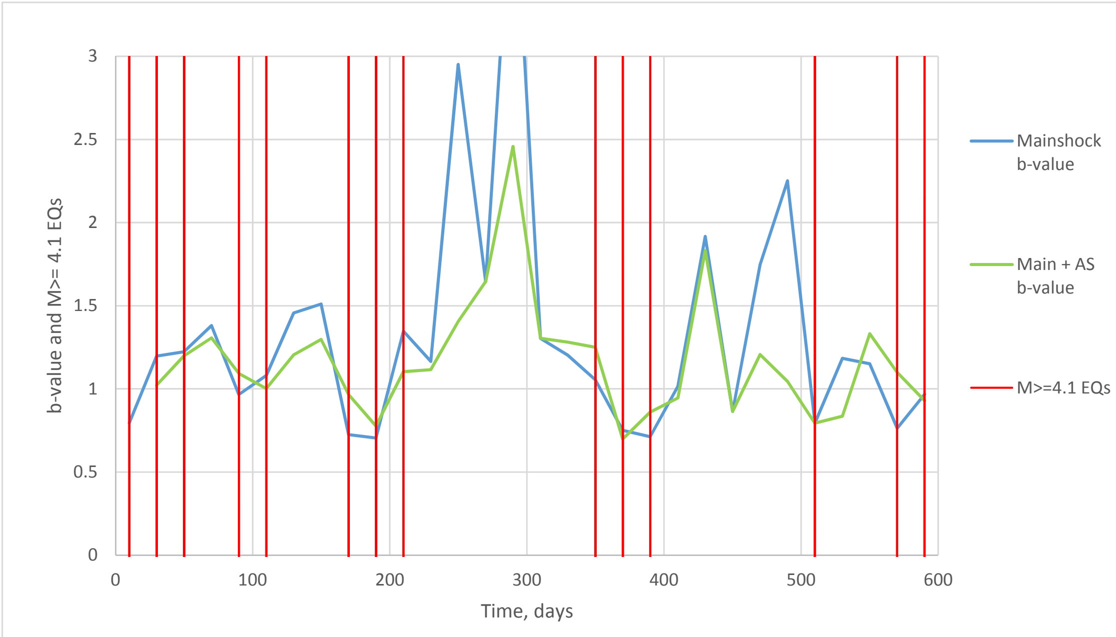

Fig. 12. – Calculated b-values vs time for simulated mainshocks and for mainshocks + aftershocks, with M≥4.1 earthquakes shown as vertical red lines.

4. Conclusions

If earthquakes are causally related to underground injection of saline water, occurrences of those earthquakes in time and space will be affected by pumping volumes and pressures, and by crustal characteristics in the geologic unit used for disposal. The observations of characteristics of small-to-moderate earthquakes in Oklahoma, and the modeling of those same characteristics with simple crustal pore-pressure calculations and a simple fault rupture failure model, lead to the following conclusions.

The observation of moderate (**M**≥4.9) earthquakes occurring at the edge of seismicity is consistent with crustal stress being released by prior earthquakes at the centers of clusters (near injection wells), and with pore pressure changes migrating to previously undisturbed parts of the crust. These previously undisturbed parts of the crust will have earthquakes triggered on faults that are favorably oriented with respect to crustal stresses, when pore pressure changes are sufficient to induce slip on those faults.

The occurrence in time of earthquakes with m≥4.2 following a peak in b-value calculated with m≥3 earthquakes over a short time window is a correlation that can be modeled with simple crustal pore-pressure calculations and a simple fault rupture failure model. Note that the model developed here was not meant to represent any particular injection well or geologic unit into which fluids are injected. Note also that not all simulations conducted in this study showed the same degree of correlation, that the effects observed in this study may be partially due to chance, and that correlation does not imply causation, nor does it imply the ability to predict future events. However, the correlation observed in the simple model results presented here illustrate that characteristics of seismicity in Oklahoma can be replicated with a simple crustal pore-pressure calculation and a simple fault rupture failure model.

Note finally that, if earthquakes are related to underground injection wells and disposal of fluids, the characteristics of seismicity in that region will depend on the rates, pressures, total volumes, and time period over which the injection wells are operating, among many other things. If these rates, pressures and total volumes change in time, the characteristics of related seismicity can be expected to change as a result.

5. References

[1] Oklahoma Corporation Commission (2016a): Media Advisory—Fairview Area Earthquakes. Oklahoma Corp. Comm. News release on 1/13/2016.

[2] Oklahoma Corporation Commission (2016b): Media Advisory—Regional Earthquake Response Plan for Western Oklahoma. Oklahoma Corp. Comm. News release on 2/26/2016.

[3] Ellsworth WL *et al.* (2015): Increasing seismicity in the U.S. midcontinent: Implications for earthquake hazard. *Leading Edge*, June, 618-626.

[4] Peterson MD *et al.* (2015): *Incorporating Induced Seismicity in the 2014 United States National Seismic Hazard Model—Results of 2014 Workshop and Sensitivity Studies.* US Geol. Survey Open-file Rept. 2015-1070.

[5] Peterson MD *et al* (2016): *2016 One-Year Seismic Hazard Forecast for the Central and Eastern United States from Induced and Natural Earthquakes.* US Geol. Survey Open-file Rept. 2016-1035.

[6] Weingarten M, Ge S, Godt JW, Bekins BA, and Rubinstein JL (2015): High-rate injection is associated with increase in U.S. mid-continent seismicity. *Science*, **348**(6241), 1336-1340.

[7] US Geological Survey (2016): Induced Earthquake data, available from website at http://earthquake.usgs.gov/research/induced/

[8] Peterson MD *et al.* (2014): *Documentation for the 2014 Update of the United States National Seismic Hazard Maps.* US Geol. Survey Open-file Rept. 2014-1091.

[9] Oklahoma Geological Survey/University of Oklahoma (2016): Earthquake catalog data, available from www.ou.edu/content/ogs/research/earthquakes/catalogs.html

[10] US Geological Survey (2016): Earthquake catalog data, available from "Search Earthquake Archives" website at http://earthquake.usgs.gov/earthquakes/browse/significant.php.

[11] Mena B, Wiemer S, and Bachmann C (2013): Building robust models to forecast the induced seismicity related to geothermal reservoir enhancement, *Bulletin Seism. Society America*, **103**(1), 383-393.

[12] Dost B, Goutbeek F, Eck TV, and Kraaijpoel D (2012): *Monitoring induced seismicity in the north of the Netherlands: status report 2010,* Technical Report, Koninklijk Nederlands Meterologisch.

[13] Benz HM, McMahon ND, Aster RC, McNamara DE, and Harris DB (2015): Hundreds of Earthquake per Day: The 2014 Guthrie, Oklahoma, Earthquake Sequence. *Seism. Res. Ltrs*, **86**(5), 1318-1325.

[14] Convertito V, Maercklin N, Sharma N and Zollo A (2012): From induced seismicity to direct time-dependent seismic hazard, *Bulletin Seism. Society America*, **102**(6), 2563-2573.

[15] Martinez-Garzon P, Kwiatek G, Sone H, Bohnhoff M, Dresen G, and Hartline C (2014): Spatiotemporal changes, faulting regimes, and source parameters of induced seismicity: a case study from The Geysers geotermal field, *Journal Geophysical Research Solid Earth*, **119**, 8378-8396.